Title

Measurement of elliptic flow of light nuclei at sNN =200, 62.4, 39, 27, 19.6, 11.5, and 7.7 GeV at the BNL Relativistic Heavy Ion Collider

Authors

Adamczyk, L
Adkins, JK
Agakishiev, G
et al.

Peer reviewed

Measurement of elliptic flow of light nuclei at $\sqrt{s_{NN}} = 200$, 62.4, 39, 27, 19.6, 11.5, and 7.7 GeV at the BNL Relativistic Heavy Ion Collider

L. Adamczyk,[1] J. K. Adkins,[20] G. Agakishiev,[18] M. M. Aggarwal,[31] Z. Ahammed,[49] I. Alekseev,[16] A. Aparin,[18] D. Arkhipkin,[3] E. C. Aschenauer,[3] A. Attri,[31] G. S. Averichev,[18] X. Bai,[7] V. Bairathi,[27] R. Bellwied,[45] A. Bhasin,[17] A. K. Bhati,[31] P. Bhattarai,[44] J. Bielcik,[10] J. Bielcikova,[11] L. C. Bland,[3] I. G. Bordyuzhin,[16] J. Bouchet,[19] J. D. Brandenburg,[37] A. V. Brandin,[26] I. Bunzarov,[18] J. Butterworth,[37] H. Caines,[53] M. Calderón de la Barca Sánchez,[5] J. M. Campbell,[29] D. Cebra,[5] I. Chakaberia,[3] P. Chaloupka,[10] Z. Chang,[43] A. Chatterjee,[49] S. Chattopadhyay,[49] J. H. Chen,[40] X. Chen,[22] J. Cheng,[46] M. Cherney,[9] W. Christie,[3] G. Contin,[23] H. J. Crawford,[4] S. Das,[13] L. C. De Silva,[9] R. R. Debbe,[3] T. G. Dedovich,[18] J. Deng,[39] A. A. Derevschikov,[33] B. di Ruzza,[3] L. Didenko,[3] C. Dilks,[32] X. Dong,[23] J. L. Drachenberg,[48] J. E. Draper,[5] C. M. Du,[22] L. E. Dunkelberger,[6] J. C. Dunlop,[3] L. G. Efimov,[18] J. Engelage,[4] G. Eppley,[37] R. Esha,[6] O. Evdokimov,[8] O. Eyser,[3] R. Fatemi,[20] S. Fazio,[3] P. Federic,[11] J. Fedorisin,[18] Z. Feng,[7] P. Filip,[18] Y. Fisyak,[3] C. E. Flores,[5] L. Fulek,[1] C. A. Gagliardi,[43] D. Garand,[34] F. Geurts,[37] A. Gibson,[48] M. Girard,[50] L. Greiner,[23] D. Grosnick,[48] D. S. Gunarathne,[42] Y. Guo,[38] S. Gupta,[17] A. Gupta,[17] W. Guryn,[3] A. I. Hamad,[19] A. Hamed,[43] R. Haque,[27] J. W. Harris,[53] L. He,[34] S. Heppelmann,[5] S. Heppelmann,[32] A. Hirsch,[34] G. W. Hoffmann,[44] S. Horvat,[53] T. Huang,[28] X. Huang,[46] B. Huang,[8] H. Z. Huang,[6] P. Huck,[7] T. J. Humanic,[29] G. Igo,[6] W. W. Jacobs,[15] H. Jang,[21] A. Jentsch,[44] J. Jia,[3] K. Jiang,[38] E. G. Judd,[4] S. Kabana,[19] D. Kalinkin,[15] K. Kang,[46] K. Kauder,[51] H. W. Ke,[3] D. Keane,[19] A. Kechechyan,[18] Z. H. Khan,[8] D. P. Kikoła,[50] I. Kisel,[12] A. Kisiel,[50] L. Kochenda,[26] D. D. Koetke,[48] L. K. Kosarzewski,[50] A. F. Kraishan,[42] P. Kravtsov,[26] K. Krueger,[2] L. Kumar,[31] M. A. C. Lamont,[3] J. M. Landgraf,[3] K. D. Landry,[6] J. Lauret,[3] A. Lebedev,[3] R. Lednicky,[18] J. H. Lee,[3] X. Li,[42] C. Li,[38] X. Li,[38] Y. Li,[46] W. Li,[40] T. Lin,[15] M. A. Lisa,[29] F. Liu,[7] T. Ljubicic,[3] W. J. Llope,[51] M. Lomnitz,[19] R. S. Longacre,[3] X. Luo,[7] R. Ma,[3] G. L. Ma,[40] Y. G. Ma,[40] L. Ma,[40] N. Magdy,[41] R. Majka,[53] A. Manion,[23] S. Margetis,[19] C. Markert,[44] H. S. Matis,[23] D. McDonald,[45] S. McKinzie,[23] K. Meehan,[5] J. C. Mei,[39] N. G. Minaev,[33] S. Mioduszewski,[43] D. Mishra,[27] B. Mohanty,[27] M. M. Mondal,[43] D. A. Morozov,[33] M. K. Mustafa,[23] B. K. Nandi,[14] Md. Nasim,[6] T. K. Nayak,[49] G. Nigmatkulov,[26] T. Niida,[51] L. V. Nogach,[33] S. Y. Noh,[21] J. Novak,[25] S. B. Nurushev,[33] G. Odyniec,[23] A. Ogawa,[3] K. Oh,[35] V. A. Okorokov,[26] D. Olvitt Jr.,[42] B. S. Page,[3] R. Pak,[3] Y. X. Pan,[6] Y. Pandit,[8] Y. Panebratsev,[18] B. Pawlik,[30] H. Pei,[7] C. Perkins,[4] P. Pile,[3] J. Pluta,[50] K. Poniatowska,[50] J. Porter,[23] M. Posik,[42] A. M. Poskanzer,[23] N. K. Pruthi,[31] J. Putschke,[51] H. Qiu,[23] A. Quintero,[19] S. Ramachandran,[20] R. Raniwala,[36] S. Raniwala,[36] R. L. Ray,[44] H. G. Ritter,[23] J. B. Roberts,[37] O. V. Rogachevskiy,[18] J. L. Romero,[5] L. Ruan,[3] J. Rusnak,[11] O. Rusnakova,[10] N. R. Sahoo,[43] P. K. Sahu,[13] I. Sakrejda,[23] S. Salur,[23] J. Sandweiss,[53] A. Sarkar,[14] J. Schambach,[44] R. P. Scharenberg,[34] A. M. Schmah,[23] W. B. Schmidke,[3] N. Schmitz,[24] J. Seger,[9] P. Seyboth,[24] N. Shah,[40] E. Shahaliev,[18] P. V. Shanmuganathan,[19] M. Shao,[38] M. K. Sharma,[17] B. Sharma,[31] W. Q. Shen,[40] Z. Shi,[23] S. S. Shi,[7] Q. Y. Shou,[40] E. P. Sichtermann,[23] R. Sikora,[1] M. Simko,[11] S. Singha,[19] M. J. Skoby,[15] N. Smirnov,[53] D. Smirnov,[3] W. Solyst,[15] L. Song,[45] P. Sorensen,[3] H. M. Spinka,[2] B. Srivastava,[34] T. D. S. Stanislaus,[48] M. Stepanov,[34] R. Stock,[12] M. Strikhanov,[26] B. Stringfellow,[34] M. Sumbera,[11] B. Summa,[32] X. M. Sun,[7] Z. Sun,[22] Y. Sun,[38] B. Surrow,[42] D. N. Svirida,[16] Z. Tang,[38] A. H. Tang,[3] T. Tarnowsky,[25] A. Tawfik,[52] J. Thäder,[23] J. H. Thomas,[23] A. R. Timmins,[45] D. Tlusty,[37] T. Todoroki,[3] M. Tokarev,[18] S. Trentalange,[6] R. E. Tribble,[43] P. Tribedy,[3] S. K. Tripathy,[13] O. D. Tsai,[6] T. Ullrich,[3] D. G. Underwood,[2] I. Upsal,[29] G. Van Buren,[3] G. van Nieuwenhuizen,[3] M. Vandenbroucke,[42] R. Varma,[14] A. N. Vasiliev,[33] R. Vertesi,[11] F. Videbæk,[3] S. Vokal,[18] S. A. Voloshin,[51] A. Vossen,[15] Y. Wang,[7] G. Wang,[6] J. S. Wang,[22] H. Wang,[3] Y. Wang,[46] F. Wang,[34] G. Webb,[3] J. C. Webb,[3] L. Wen,[6] G. D. Westfall,[25] H. Wieman,[23] S. W. Wissink,[15] R. Witt,[47] Y. Wu,[19] Z. G. Xiao,[46] W. Xie,[34] G. Xie,[38] K. Xin,[37] H. Xu,[22] Z. Xu,[3] J. Xu,[7] Y. F. Xu,[40] Q. H. Xu,[39] N. Xu,[23] Y. Yang,[7] S. Yang,[38] C. Yang,[38] Y. Yang,[22] Y. Yang,[28] Q. Yang,[38] Z. Ye,[8] Z. Ye,[8] P. Yepes,[37] L. Yi,[53] K. Yip,[3] I.-K. Yoo,[35] N. Yu,[7] H. Zbroszczyk,[50] W. Zha,[38] J. Zhang,[39] Y. Zhang,[38] X. P. Zhang,[46] Z. Zhang,[40] J. B. Zhang,[7] S. Zhang,[38] S. Zhang,[40] J. Zhang,[22] J. Zhao,[34] C. Zhong,[40] L. Zhou,[38] X. Zhu,[46] Y. Zoulkarneeva,[18] and M. Zyzak[12]

(STAR Collaboration)

[1]*AGH University of Science and Technology, FPACS, Cracow 30-059, Poland*
[2]*Argonne National Laboratory, Argonne, Illinois 60439, USA*
[3]*Brookhaven National Laboratory, Upton, New York 11973, USA*
[4]*University of California, Berkeley, California 94720, USA*
[5]*University of California, Davis, California 95616, USA*
[6]*University of California, Los Angeles, California 90095, USA*
[7]*Central China Normal University, Wuhan, Hubei 430079, China*
[8]*University of Illinois at Chicago, Chicago, Illinois 60607, USA*
[9]*Creighton University, Omaha, Nebraska 68178, USA*
[10]*Czech Technical University in Prague, FNSPE, Prague, 115 19, Czech Republic*
[11]*Nuclear Physics Institute AS CR, 250 68 Prague, Czech Republic*
[12]*Frankfurt Institute for Advanced Studies FIAS, Frankfurt 60438, Germany*
[13]*Institute of Physics, Bhubaneswar 751005, India*
[14]*Indian Institute of Technology, Mumbai 400076, India*
[15]*Indiana University, Bloomington, Indiana 47408, USA*

[16]*Alikhanov Institute for Theoretical and Experimental Physics, Moscow 117218, Russia*
[17]*University of Jammu, Jammu 180001, India*
[18]*Joint Institute for Nuclear Research, Dubna, 141 980, Russia*
[19]*Kent State University, Kent, Ohio 44242, USA*
[20]*University of Kentucky, Lexington, Kentucky, 40506-0055, USA*
[21]*Korea Institute of Science and Technology Information, Daejeon 305-701, Korea*
[22]*Institute of Modern Physics, Chinese Academy of Sciences, Lanzhou, Gansu 730000, China*
[23]*Lawrence Berkeley National Laboratory, Berkeley, California 94720, USA*
[24]*Max-Planck-Institut fur Physik, Munich 80805, Germany*
[25]*Michigan State University, East Lansing, Michigan 48824, USA*
[26]*National Research Nuclear Univeristy MEPhI, Moscow 115409, Russia*
[27]*National Institute of Science Education and Research, Bhubaneswar 751005, India*
[28]*National Cheng Kung University, Tainan 70101, Taiwan*
[29]*Ohio State University, Columbus, Ohio 43210, USA*
[30]*Institute of Nuclear Physics PAN, Cracow 31-342, Poland*
[31]*Panjab University, Chandigarh 160014, India*
[32]*Pennsylvania State University, University Park, Pennsylvania 16802, USA*
[33]*Institute of High Energy Physics, Protvino 142281, Russia*
[34]*Purdue University, West Lafayette, Indiana 47907, USA*
[35]*Pusan National University, Pusan 46241, Korea*
[36]*University of Rajasthan, Jaipur 302004, India*
[37]*Rice University, Houston, Texas 77251, USA*
[38]*University of Science and Technology of China, Hefei, Anhui 230026, China*
[39]*Shandong University, Jinan, Shandong 250100, USA*
[40]*Shanghai Institute of Applied Physics, Chinese Academy of Sciences, Shanghai 201800, China*
[41]*State University Of New York, Stony Brook, New York 11794, USA*
[42]*Temple University, Philadelphia, Pennsylvania 19122, USA*
[43]*Texas A&M University, College Station, Texas 77843, USA*
[44]*University of Texas, Austin, Texas 78712, USA*
[45]*University of Houston, Houston, Texas 77204, USA*
[46]*Tsinghua University, Beijing 100084, China*
[47]*United States Naval Academy, Annapolis, Maryland, 21402, USA*
[48]*Valparaiso University, Valparaiso, Indiana 46383, USA*
[49]*Variable Energy Cyclotron Centre, Kolkata 700064, India*
[50]*Warsaw University of Technology, Warsaw 00-661, Poland*
[51]*Wayne State University, Detroit, Michigan 48201, USA*
[52]*World Laboratory for Cosmology and Particle Physics (WLCAPP), Cairo 11571, Egypt*
[53]*Yale University, New Haven, Connecticut 06520, USA*

We present measurements of second-order azimuthal anisotropy (v_2) at midrapidity ($|y| < 1.0$) for light nuclei d, t, ^{3}He (for $\sqrt{s_{NN}}$ = 200, 62.4, 39, 27, 19.6, 11.5, and 7.7 GeV) and antinuclei $\overline{d}$ ($\sqrt{s_{NN}}$ = 200, 62.4, 39, 27, and 19.6 GeV) and $^3\overline{\text{He}}$ ($\sqrt{s_{NN}}$ = 200 GeV) in the STAR (Solenoidal Tracker at RHIC) experiment. The v_2 for these light nuclei produced in heavy-ion collisions is compared with those for p and $\overline{p}$. We observe mass ordering in nuclei $v_2(p_T)$ at low transverse momenta ($p_T < 2.0$ GeV/c). We also find a centrality dependence of v_2 for d and $\overline{d}$. The magnitude of v_2 for t and ^{3}He agree within statistical errors. Light-nuclei v_2 are compared with predictions from a blast-wave model. Atomic mass number (A) scaling of light-nuclei $v_2(p_T)$ seems to hold for $p_T/A < 1.5$ GeV/c. Results on light-nuclei v_2 from a transport-plus-coalescence model are consistent with the experimental measurements.

I. INTRODUCTION

One of the main goals of high-energy heavy-ion collision experiments is to study phase structures in the QCD phase diagram [1,2]. With this purpose, the Relativistic Heavy Ion Collider (RHIC) has finished the first phase of the Beam Energy Scan (BES) program [3–9]. It was found that the identified hadron v_2 shows approximate number-of-constituent-quark (NCQ) scaling at high p_T at the higher beam energies. This scaling behavior is an expected signature of partonic collectivity via quark coalescence in the strongly interacting medium of quarks and gluons formed in heavy-ion collisions [10–16]. Such a scaling behavior also suggests partonic

coalescence to be a mechanism for hadron formation [10,11,17]. In a relativistic heavy-ion collision, light (anti) nuclei can be formed by coalescence of produced (anti) nucleons or from transported nucleons [18–20]. The binding energies of light nuclei are very small ($\sim$ a few MeV). Therefore, it seems more probable that light nuclei may be produced at a later stage of the evolution. This phenomenon is called final-state coalescence [18,21]. The coalescence probability of two nucleons is related to the local nucleon density [18,19,22]. Since the coalescence mechanism works best at the low-density limit, low relative production of nucleons in heavy-ion collisions offers an ideal situation to study light-nuclei production via coalescence. Measurements of azimuthal anisotropy of light nuclei offers a tool to understand the light-nuclei production mechanism and freeze-out properties at a later stage of the evolution. Unlike the case of quark coalescence, in a nucleon coalescence, the momentum space distributions of both the constituents and the products are measurable in heavy-ion collision experiments.

Prior measurements of elliptic flow (v_2) of light nuclei have been carried out at the top RHIC energy ($\sqrt{s_{NN}} = 200$ GeV) by the PHENIX [23] and the STAR [24,25] experiments. The PHENIX Collaboration has measured the v_2 of deuterons (d) and antideuterons ($\bar{d}$) at intermediate transverse momenta ($1.1 < p_T < 4.5$ GeV/c). How the v_2 of these light nuclei scale with those of (anti) protons also has been reported [23]. The STAR collaboration has measured the v_2 of d, $\bar{d}$, ^{3}He, and $^3\overline{\text{He}}$ in Au + Au collisions at $\sqrt{s_{NN}} = 200$ GeV in the years 2004 [24] and 2007 [25].

In this work we expand upon previous studies with a detailed investigation on the energy and centrality dependence of v_2 of light nuclei with more event statistics. During the BES program, the STAR experiment has taken data over a wide range of collision energies from $\sqrt{s_{NN}} = 7.7$ GeV to 200 GeV. In this paper we present the measurement of v_2 at midrapidity ($|y| < 1.0$) for light nuclei d, t, ^{3}He ($\sqrt{s_{NN}} = 200$, 62.4, 39, 27, 19.6, 11.5, and 7.7 GeV), and antinuclei $\bar{d}$ ($\sqrt{s_{NN}} = 200$, 62.4, 39, 27, and 19.6 GeV) and $^3\overline{\text{He}}$ ($\sqrt{s_{NN}} = 200$ GeV).

The paper is organized as follows: Section II briefly describes the experimental setup, the detectors, and the particle (and light nuclei) identification (PID) techniques. The centrality definition, event selection, event plane reconstruction, and the event plane resolution correction are also discussed, along with the extraction procedure of light-nuclei v_2. Presented in Sec. III are the v_2 results for minimum-bias collisions, the centrality dependence, and a physical interpretation of the results. A comparison between light-nuclei v_2 measured in this experiment and those calculated from blast-wave and transport-plus-coalescence models is also shown. Section IV summarizes the physics observations and discusses the main conclusions from the results.

II. EXPERIMENTAL SETUP

STAR is a multipurpose experiment at the RHIC facility at Brookhaven National Laboratory. It consists of a longitudinally oriented (beam direction) solenoidal magnet and a collection of detectors for triggering, PID, and event categorization [27]. The main detectors used for this analysis are the time projection chamber (TPC) [28] and the time of flight (TOF) detector [29]. The following subsections briefly describe their operations and PID techniques.

A. Time projection chamber measurements

The TPC is the primary tracking device in the STAR experiment which uses ionization in a large gas volume to detect trajectories of charged particles. Curvature in the solenoidal field enables determination of the charge sign and rigidity (momentum/charge). The TPC has full azimuthal coverage and a uniform pseudorapidity range of $|\eta| < 1.0$ [28]. The TPC can record up to 45 hit positions and specific ionization energy loss (dE/dx) samples along tracks. Truncated means of the dE/dx samples are used for PID by comparing to theoretical expectations, using improved Bethe–Bloch functions [26], at the measured rigidities to characterize the probability for being any particular species. PID consequently allows deduction of the particles' charges and momenta. A representative plot of measured track dE/dx versus rigidity is shown in Fig. 1(a) for minimum-bias (defined later) Au + Au collisions at $\sqrt{s_{NN}} = 19.6$ GeV. The theoretical curves are shown as solid lines. Primary collision vertices are found through fits involving candidate global tracks, and a typical central collision at the top RHIC energy (with perhaps $\sim$1000 reconstructed tracks) may achieve a vertex position resolution of $\sim$350 μm. These global tracks are then refitted by using their vertex as a constraint to create a collection of primary tracks.

B. Time of flight measurements

The TOF detector [29] in STAR uses multigap resistive plate chambers (MRPCs) and was fully installed in the year 2010. It covers 2π in azimuth within the pseudorapidity interval $|\eta| < 0.94$. The TOF detector and the vertex position detector (VPD) [30] measure the time interval t over which a particle travels from the primary collision vertex to a read-out cell of the TOF detector. This time-interval information is combined with the total path length S measured by the TPC to provide the inverse velocity, $1/\beta$, via $1/\beta = ct/S$, where c is the speed of light. The track mass-squared is then given by $m^2 = p^2(1/\beta^2 - 1)$. For collision energies below $\sqrt{s_{NN}} = 39$ GeV the VPD efficiency is too low to use in every event. Instead, for these data sets a start time for each collision is inferred by working backwards from the TOF-measured stop times of a very limited selection of particles which are very cleanly identified in the TPC. The total time interval resolution obtained of 90–110 ps results in PID capabilities that are complementary to those from the TPC dE/dx at low momenta and also extend to momenta of several GeV. A representative plot of m^2 as a function of the particle momentum is shown in Fig. 1(b) for minimum-bias Au + Au collisions at $\sqrt{s_{NN}} = 19.6$ GeV. As the mass of a particle is a constant quantity, we expect horizontal bands for individual (anti) nuclei as shown by the dotted lines in Fig. 1(b). The large background at low p_T (<1.0 GeV/c) is the result of mismatched tracks in TOF. However, this does not affect the measurement of light nuclei because the TOF detector has been used to identify light nuclei in the high p_T (>1.0 GeV/c) region. The matched tracks in TOF corresponds to 70% to
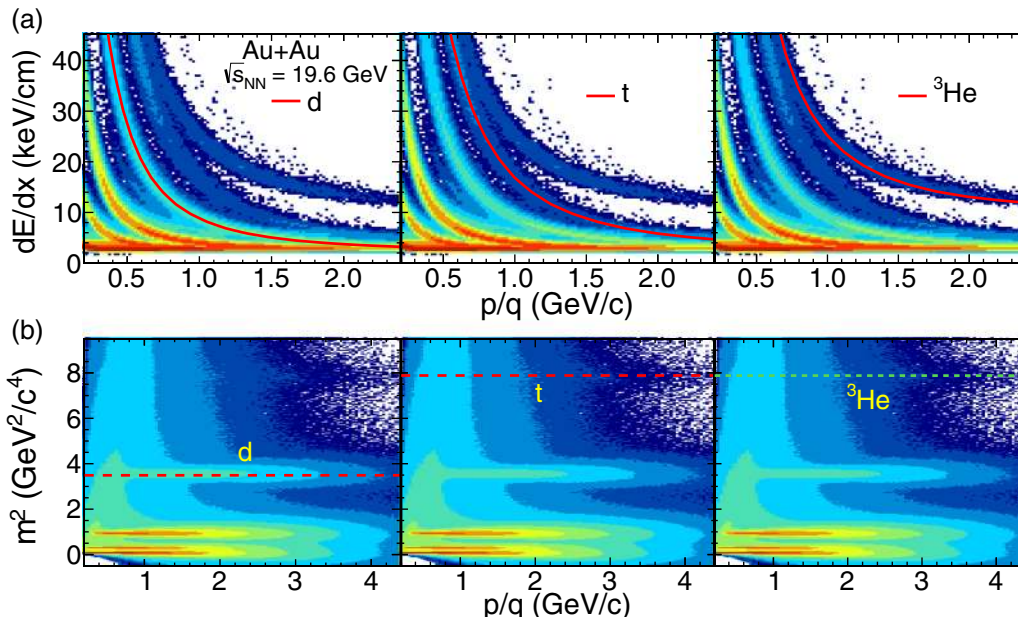
FIG. 1. (a) Specific energy loss (dE/dx) as a function of rigidity (momentum/charge). Theoretical dE/dx expectations, by using the model in Ref. [26] of d, t, ^{3}He are shown by solid curves. (b) Mass squared (m^2) as a function of momentum for midrapidity charged particles. The dotted lines correspond to m^2 of different nuclei. Both results are from minimum-bias Au + Au collisions at $\sqrt{s_{NN}} = 19.6$ GeV.

75% of the total tracks measured by the TPC. This matching efficiency is higher at lower beam energies due to low detector occupancy. We selected individual nuclei by using the m^2 which lie within 3σ from the constant mean (dotted line).

C. Trigger and event selection

The minimum-bias events for all of the collision energies are based on a coincidence of the signals from the zero-degree calorimeters (ZDCs) [31], VPD, and/or beam-beam counters (BBCs) [32]. Due to larger beam emittance at lower collision energies, (Au + Au)-triggered events are contaminated with Au + beam-pipe events. The radius of the beam pipe going through the center of the TPC is 3.95 cm. Therefore, such Au + beam-pipe events are removed by requiring the primary vertex position to be within a transverse radius of less than 2 cm in the XY plane [4]. The z position of the primary vertices (vertex z) is limited to the values listed in Table I [4] to ensure good-quality events.

Furthermore, an extensive quality assurance of the events was performed based on the mean transverse momenta, the

TABLE I. The vertex-z acceptance and total number of minimum-bias (MB) events for each energy ($\sqrt{s_{NN}}$).

$\sqrt{s_{NN}}$ (GeV)	vertex z (cm)	MB events ($\times 10^6$)
200	|vertex z| < 30	241
62.4	|vertex z| < 40	62
39	|vertex z| < 40	119
27	|vertex z| < 70	60
19.6	|vertex z| < 70	33
11.5	|vertex z| < 50	11
7.7	|vertex z| < 70	4

mean vertex position, the mean interaction rate, and the mean multiplicity in the detector. Run periods were removed if one of those quantities was more than 3σ away from the global mean value. The total number of minimum-bias events used in this analysis after these quality assurance cuts for each collision energy are shown in Table I.

D. Centrality definition

The centrality of each event is defined based on the uncorrected charged particle multiplicity ($dN_{\text{events}}/dN_{\text{charge}}^{\text{raw}}$) distribution, where N_{events} is the number of events and $N_{\text{charge}}^{\text{raw}}$ is the number of charged particles measured within $|\eta| < 0.5$ [4]. Thus, for example, 0%–5% central events correspond to the events in the top 5% of the multiplicity distribution. The charged particle multiplicity distributions for all energies can be described by a two-component model [33]. The two-component model is a Glauber Monte Carlo simulation in which the multiplicity per unit pseudorapidity ($dN_{\text{charge}}/d\eta$) depends on the two components; namely, number of participant nucleons (N_{part}) and number of binary collisions (N_{coll}):

$$\frac{dN_{\text{charge}}}{d\eta} = n_{pp}\left[(1-x)\frac{N_{\text{part}}}{2} + xN_{\text{coll}}\right]. \quad (1)$$

The fitting parameter n_{pp} is the $dN_{\text{charge}}/d\eta$ in minimum-bias p + p collisions and x is the fraction of charged particles produced from the hard component. The centrality class is defined by calculating the fraction of the total cross section obtained from the simulated multiplicity. Due to trigger inefficiencies, many of the most-peripheral events were not recorded. This results in a significant difference between the measured distribution of charged particle multiplicities and the Glauber Monte Carlo (MC) simulation for peripheral collisions. When determining v_2 in a bin of multiplicity wide

enough to see variation in the trigger inefficiency across the bin (e.g., for a minimum-bias measurement), it is necessary to compensate for this variation by weighting particle yields in each event by the inverse of the trigger efficiency at that event's multiplicity [4]. The correction is about 5% for the peripheral (70%–80%) events, and becomes negligible for central events. However, the corrections are severe for 80%–100% central events. Therefore, 80%–100% central events are not included in the current analysis, and minimum bias is defined for all data presented here as 0%–80%. In addition to the trigger inefficiency, two additional corrections are also applied to account for the vertex-z-dependent inefficiencies. These corrections account for the acceptance and detector inefficiencies and the time-dependent changes in $dN_{events}/dN_{charge}^{raw}$.

E. Event plane and resolution correction

The azimuthal distribution of produced particles with respect to reaction plane angle (Ψ_r) can be expressed in terms of a Fourier series,

$$\frac{dN}{d(\phi - \Psi_r)} \propto 1 + 2v_1 \cos(\phi - \Psi_r) + 2v_2 \cos[2(\phi - \Psi_r)] + \cdots, \quad (2)$$

where ϕ is the azimuthal angle of the produced particle. Ψ_r is defined as the angle between the x axis in the laboratory frame and the axis of the impact parameter. Because we cannot directly measure Ψ_r, we must use a proxy. The second-order azimuthal anisotropy or elliptic flow (v_2) is measured with respect to the second-order event plane angle (Ψ_2) instead. Ψ_2 is calculated by using the azimuthal distribution of all reconstructed primary tracks (N) [34]:

$$\Psi_2 = \frac{1}{2} \tan^{-1}\left(\frac{Q_{2,y}}{Q_{2,x}}\right). \quad (3)$$

Q_{2x} and Q_{2y} are defined as

$$Q_2 \cos(2\Psi_2) = Q_{2,x} = \sum_{i=1}^{N} w_i \cos(2\phi_i), \quad (4a)$$

$$Q_2 \sin(2\Psi_2) = Q_{2,y} = \sum_{i=1}^{N} w_i \sin(2\phi_i), \quad (4b)$$

where w_i are the weights which optimize the event plane resolution [34]. In this analysis, the weights scale with track p_T, then saturate above 2.0 GeV/c. To reduce biases due to short-range correlation, we utilize the subevent plane method [34]. In this analysis, the two subevents were defined in η windows of η^- ($-1.0 < \eta < -0.05$) and η^+ ($0.05 < \eta < 1.0$). Event plane angles are calculated within each η window, $\Psi_{2\eta^-}$ and $\Psi_{2\eta^+}$, respectively, and v_2 is calculated in each subevent by using the opposite subevent's event plane angle. The η gap ($\Delta\eta = 0.1$) between the subevents reduces the short-range nonflow contributions and avoids the self-correlation. However, long-range correlations may persist [35].

Due to the acceptance inefficiency of the detectors, the reconstructed event plane distributions are not uniform. Therefore, we apply event-by-event recenter [36] and shift [37] corrections. Finite multiplicities also restrict the degree to which the found event plane angles coincide with the true reaction plane angle. Hence, a resolution correction is applied to the observed elliptic flow (v_2^{obs}): $v_2 = v_2^{obs}/R_2$. We determine the resolution correction factor (R_2) in the η subevent plane method as follows [34]:

$$R_2 = \sqrt{\langle \cos[2(\Psi_{2\eta^+} - \Psi_{2\eta^-})] \rangle}. \quad (5)$$

The resolution as a function of centrality for η subevent planes is shown in Fig. 2 for Au + Au collisions. R_2 grows with increasing multiplicity (which is small for peripheral collisions) and with increasing v_2 (which is small for the
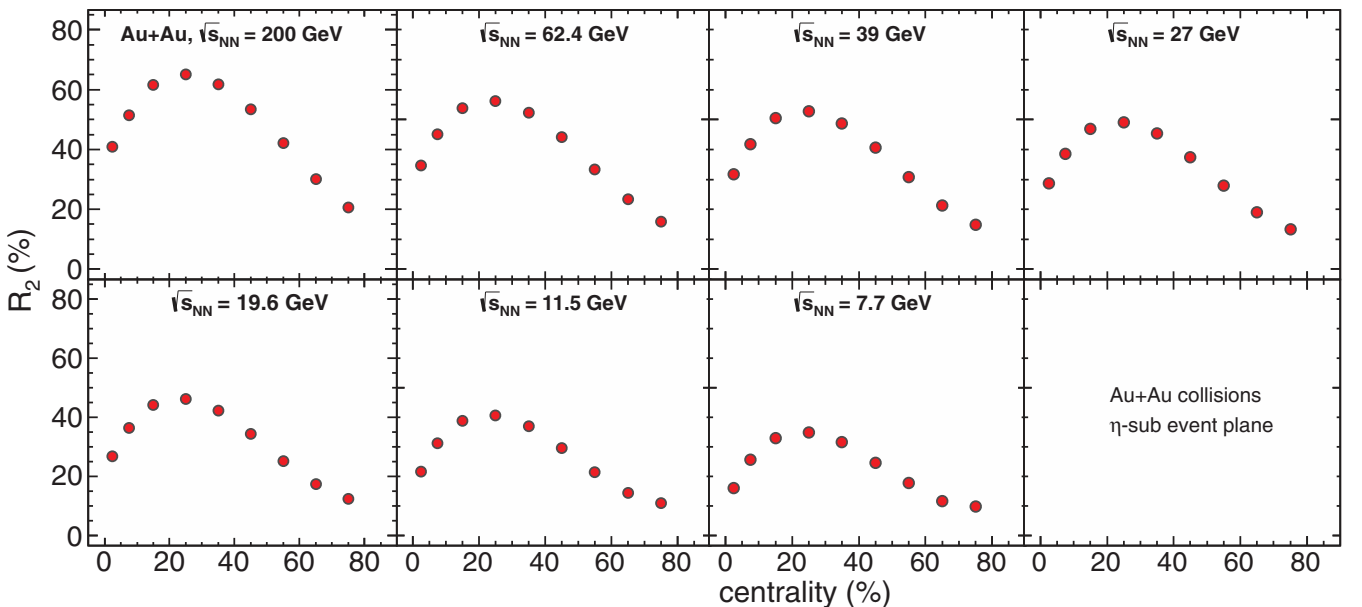

FIG. 2. Resolution correction factor R_2 of subevent planes as a function of centrality for Au + Au collisions at $\sqrt{s_{NN}} = 200$, 62.4, 39, 27, 19.6, 11.5, and 7.7 GeV.
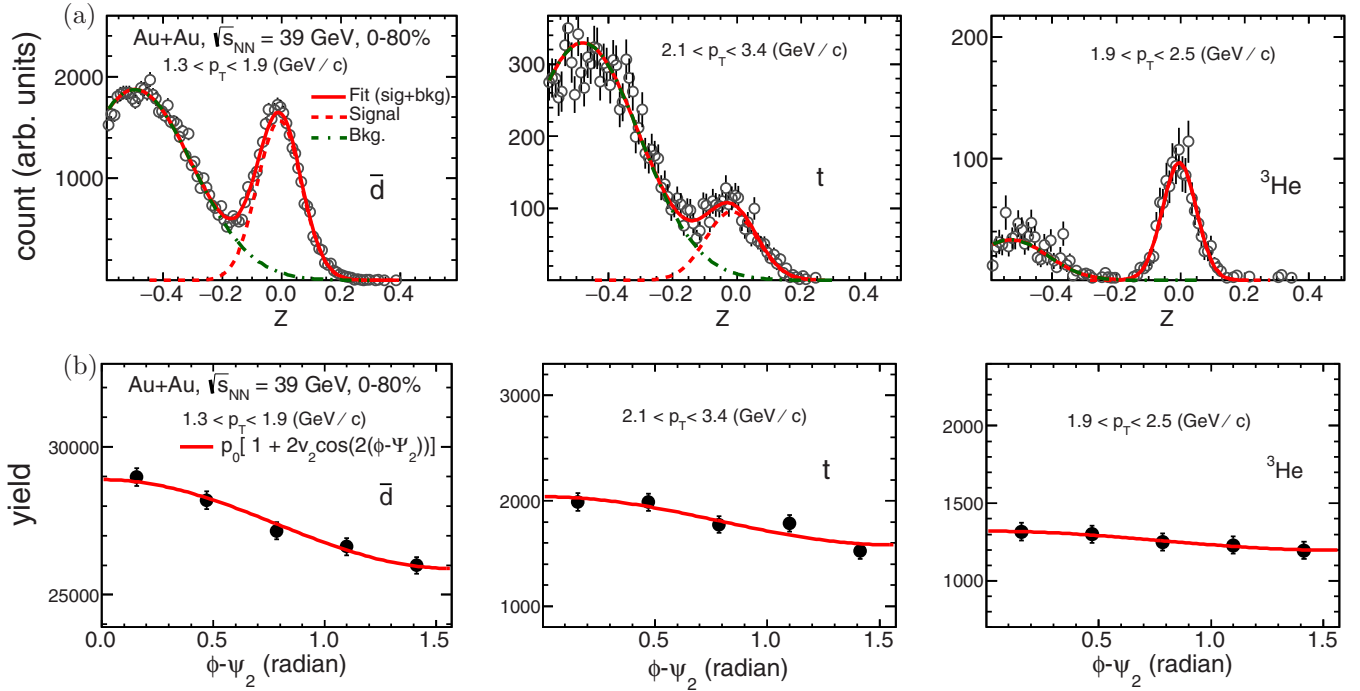
FIG. 3. (a) Z distributions for midrapidity $\overline{d}$, t, ^{3}He for $0 < (\phi - \Psi_2) < \pi/10$. The different p_T ranges are for acceptance-representative purpose. The Z distribution for each species is fit with a two-Gaussian function. One Gaussian is used to describe the Z distribution for the species of interest (dashed line), and another Gaussian is used to describe the background (dot-dashed line). (b) $(\phi - \Psi_2)$ distributions for midrapidity $\overline{d}$, t, and ^{3}He. Solid lines are fitted second-order Fourier functions. All plots use minimum-bias Au + Au collisions at $\sqrt{s_{NN}} = 39$ GeV.

most central collisions), so its value peaks in mid-central (20%–30%) collisions where neither is small.

F. Extraction of yield and v_2 of nuclei

To identify light nuclei, we define a variable Z such that

$$Z = \ln[(dE/dx)_{\text{expt}}/(dE/dx)_{\text{theory}}], \qquad (6)$$

where $(dE/dx)_{\text{expt}}$ is the energy loss of the light nuclei measured by the TPC detector in the experiment and $(dE/dx)_{\text{theory}}$ is the theoretical energy loss as obtained from the modified Bethe–Bloch formula [26]. After cutting on m^2 from the TOF [see Fig. 1(b)] to reduce backgrounds under the signals, the yields are extracted from the Z distributions in various p_T and $(\phi - \Psi_2)$ bins for each species of interest with a two-Gaussian function (one for the signal, the other for the background). Figure 3(a) shows sample Z distributions for $\overline{d}$, t, and ^{3}He, respectively, within $0 < (\phi - \Psi_2) < \pi/10$ for $1.3 < p_T < 1.9$ GeV/c, $2.1 < p_T < 3.4$ GeV/c, and $1.9 < p_T < 2.5$ GeV/c for minimum-bias Au + Au data at $\sqrt{s_{NN}} = 39$ GeV. The azimuthal angle variation of this yield is then fit with a second order Fourier function to get the elliptic flow coefficient (v_2^{obs}). Figure 3(b) shows the $(\phi - \Psi_2)$ distributions for $\overline{d}$, t, and ^{3}He for the same p_T ranges as shown for Z distributions in Fig. 3(a). Because the $(\phi - \Psi_2)$ distribution is expected to be symmetric about 0 and $\pi/2$, the data points have been folded onto 0–$\pi/2$ to reduce the statistical errors.

The fitted second-order Fourier functions are shown in Fig. 3(b). Event plane resolution correction factors are determined in each centrality bin. For v_2 integrated over

multiple centrality bins, species-yield-weighted means of the individual centrality bins' resolutions are used: $v_2 = v_2^{\text{obs}} \langle \frac{1}{R_2} \rangle$ [38].

G. Calculation of systematic uncertainty and removal of beam-pipe contaminations

We reduced light-nuclei contaminants from interactions with the beam pipe by cutting tightly on the projected distance of closest approach (DCA) to the primary vertex. Remaining contaminants from such interactions are removed statistically by fitting the DCA distribution of nuclei with that of antinuclei (which are expected to have no such background) in each $(\phi - \Psi_2)$ bin. Systematic uncertainties are determined by varying cuts used in particle identification and background rejection, and by varying fitting methods and ranges when measuring yields. The absolute magnitude of uncertainties range over 2%–5% for intermediate p_T ($1.0 < p_T < 3.0$ GeV/c) and over 5%–8% for low and high p_T.

III. RESULTS AND DISCUSSION

A. General properties of $v_2(p_T)$

Figure 4 shows the energy dependence of the v_2 of the light (anti) nuclei d, $\overline{d}$, t, ^{3}He, and $^3\overline{\text{He}}$ as a function of p_T for minimum-bias Au + Au collisions. Insufficient statistics preclude measuring differential antinuclei v_2 at several collision energies. The $v_2(p_T)$ of all light-nuclei species and antinuclei species ($\overline{d}$ at $\sqrt{s_{NN}} = 19.6 - 200$ GeV and $^3\overline{\text{He}}$ at $\sqrt{s_{NN}} = 200$ GeV) show a monotonically increasing trend

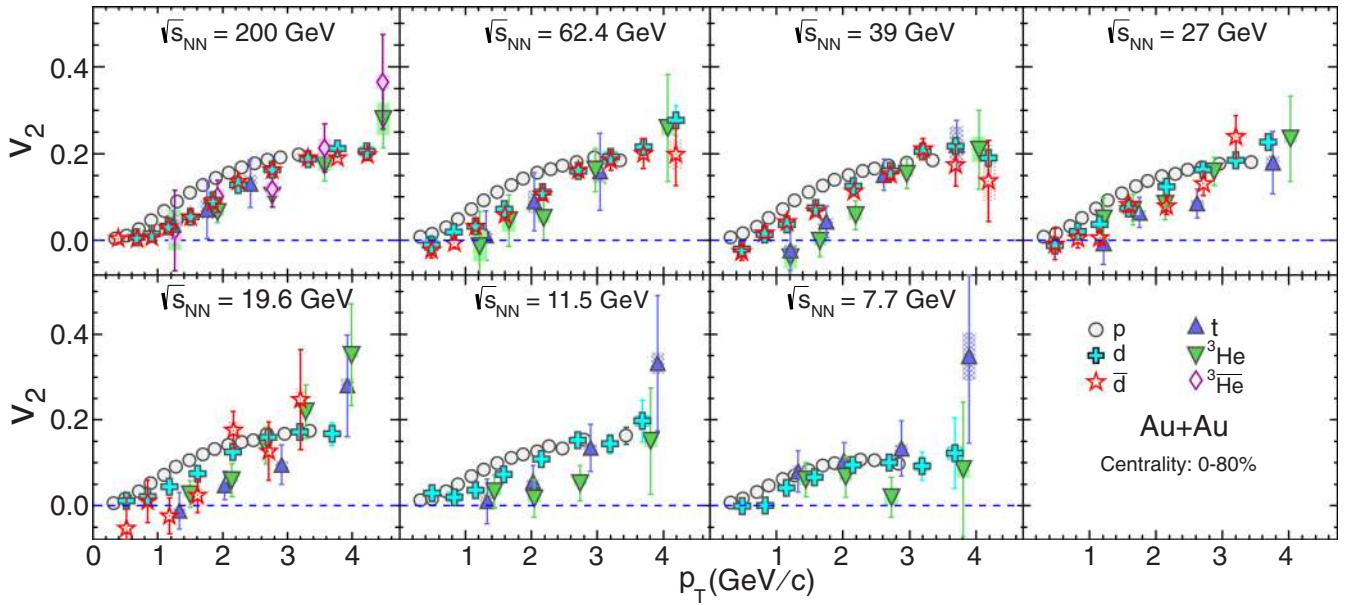FIG. 4. Midrapidity $v_2(p_T)$ for d, $\bar{d}$, t, ^{3}He, and $^3\overline{\text{He}}$ from minimum-bias Au + Au collisions at $\sqrt{s_{NN}} = 200$, 62.4, 39, 27, 19.6, 11.5, and 7.7 GeV. For comparison, proton $v_2(p_T)$ are also shown as open circles [4,9]. Lines and boxes at each marker represent statistical and systematic errors, respectively.

with increasing p_T (Fig. 4). Mass ordering of $v_2(p_T)$ for $p_T < 2.0$ GeV/c is clear in both Figs. 4 and 5, where the $v_2(p_T)$ of π^+, K_s^0, and p from Refs. [4,9] are also included (heavier species have a lower v_2 in this p_T range). Such ordering occurs naturally in a hydrodynamic plus coalescence model of heavy-ion collisions [39]. The negative v_2 observed for some (anti)-nuclei could be the result of interplay between transverse flow, modulation of transverse flow with respect to Ψ_r, and the geometry of the source.

Figure 6 presents the difference of $v_2(p_T)$ between d and $\bar{d}$ (Δv_2), along with the difference between p and $\bar{p}$ for comparison [4,9]. Statistical uncertainties are too large to draw conclusions about any collision-energy dependence, but the Δv_2 data are qualitatively consistent with the (anti) protons and the results of fitting a constant at each energy (solid lines in Fig. 6) are consistently positive: 0.0012 ± 0.0014, 0.009 ± 0.005, 0.0044 ± 0.0046, 0.017 ± 0.009, 0.024 ± 0.019 for $\sqrt{s_{NN}} = 200$, 62.4, 39, 27, and 19.6 GeV, respectively.
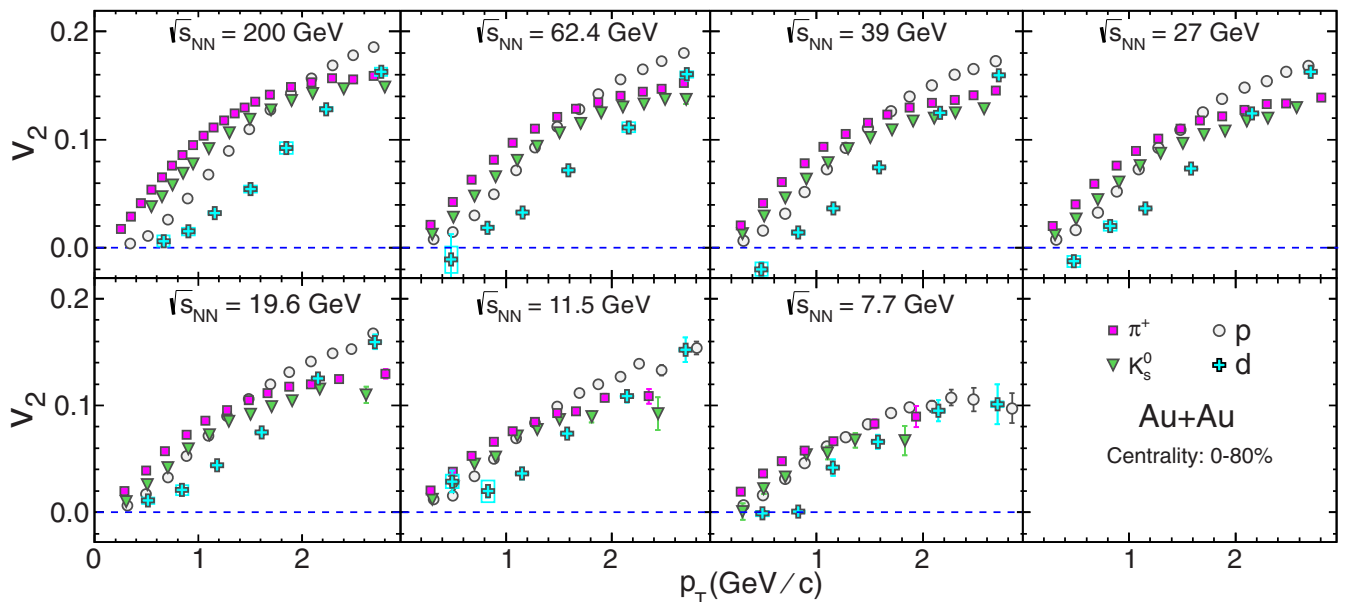

FIG. 5. Midrapidity $v_2(p_T)$ for π^+ (squares), K_s^0 (triangles), p (open circles), and d (crosses) for minimum-bias Au + Au collisions at $\sqrt{s_{NN}} = 200$, 62.4, 39, 27, 19.6, 11.5, and 7.7 GeV.
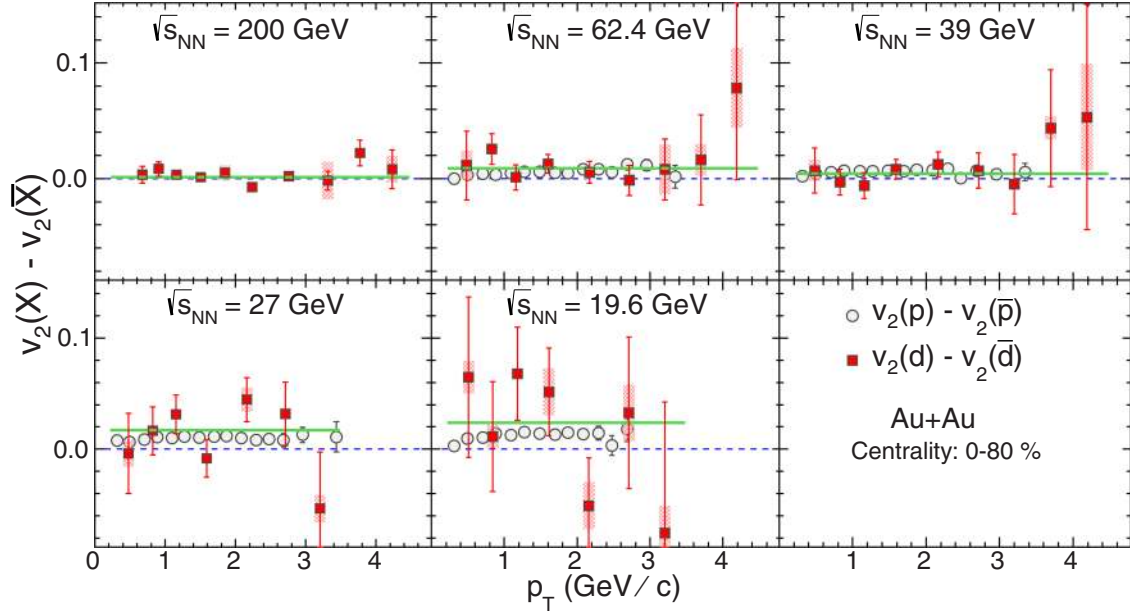
FIG. 6. The difference in v_2 of d and $\bar{d}$ as a function of p_T for minimum-bias Au + Au collisions at $\sqrt{s_{NN}} = 200$, 62.4, 39, 27, and 19.6 GeV, along with differences between p and $\bar{p}$ [4]. Solid lines correspond to constants fit to the data (see text for details).

Figure 7 shows $v_2(p_T)$ of d and $\bar{d}$ in 0%–30% and 30%–80% central events for where they could be measured in Au + Au collisions at $\sqrt{s_{NN}} = 62.4$ to 7.7 GeV. For 200 GeV v_2 are measured in three centralities: 0%–10%, 10%–40%, and 40%–80%. The observed centrality dependencies are qualitatively similar to those seen in identified hadrons [4,6], with d and $\bar{d}$ showing similar behavior for all centralities measured.

B. Blast-wave model

The nuclear fireball model was first introduced by Westfall *et al.* to explain midrapidity proton-inclusive spectra [40]. Later, Siemens and Rasmussen [41] generalized a nonrelativistic formula by Bondorf, Garpman, and Zimanyi [42]

to explain nucleons and pions as they are produced in a blast wave of an exploding fireball. The blast-wave model has evolved since then, with more parameters to describe both p_T spectra and anisotropic flow of produced particles [39,43,44]. The blast-wave parametrization modeled by the STAR Collaboration [44] has been recently used to fit the v_2 of identified particles [45]. This version of blast wave has four parameters; namely, kinetic freeze-out temperature (T), transverse expansion rapidity (ρ_0), amplitude of its azimuthal variation (ρ_a), and the variation in the azimuthal density of the source elements (s_2) [45]. The fit parameters obtained from blast-wave fits to the v_2 of identified particles are listed in Table I of Ref. [45]. We used the same blast-wave model and
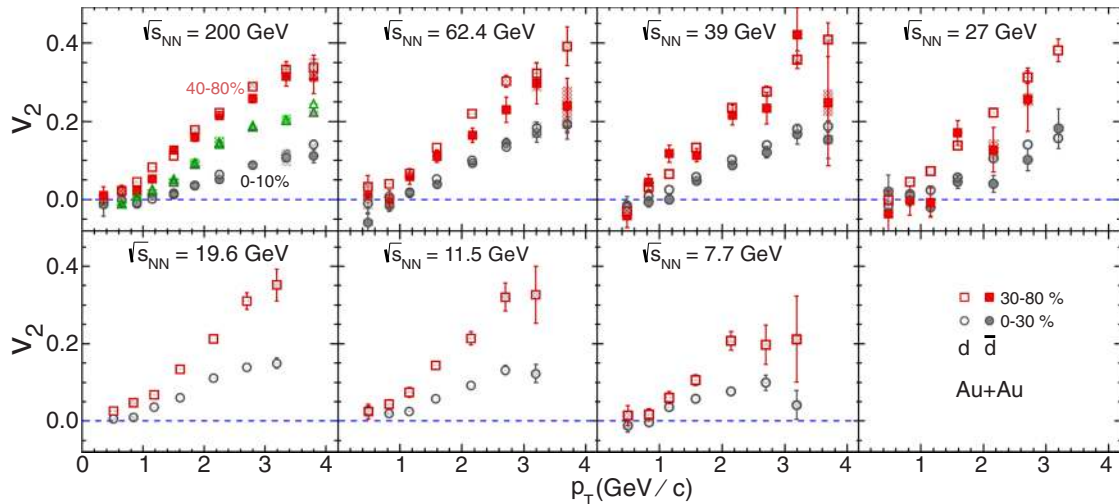

FIG. 7. Centrality dependence of midrapidity $v_2(p_T)$ of d (open markers) for Au + Au collisions at $\sqrt{s_{NN}} = 7.7$–200 GeV and $\bar{d}$ (solid markers) for $\sqrt{s_{NN}} = 27$–200 GeV. For $\sqrt{s_{NN}} = 200$ GeV, circles correspond to 0%–10%, triangles to 10%–40%, and squares to 40%–80% central events. For other collision energies, circles correspond to 0%–30% and squares to 30%–80% central events.
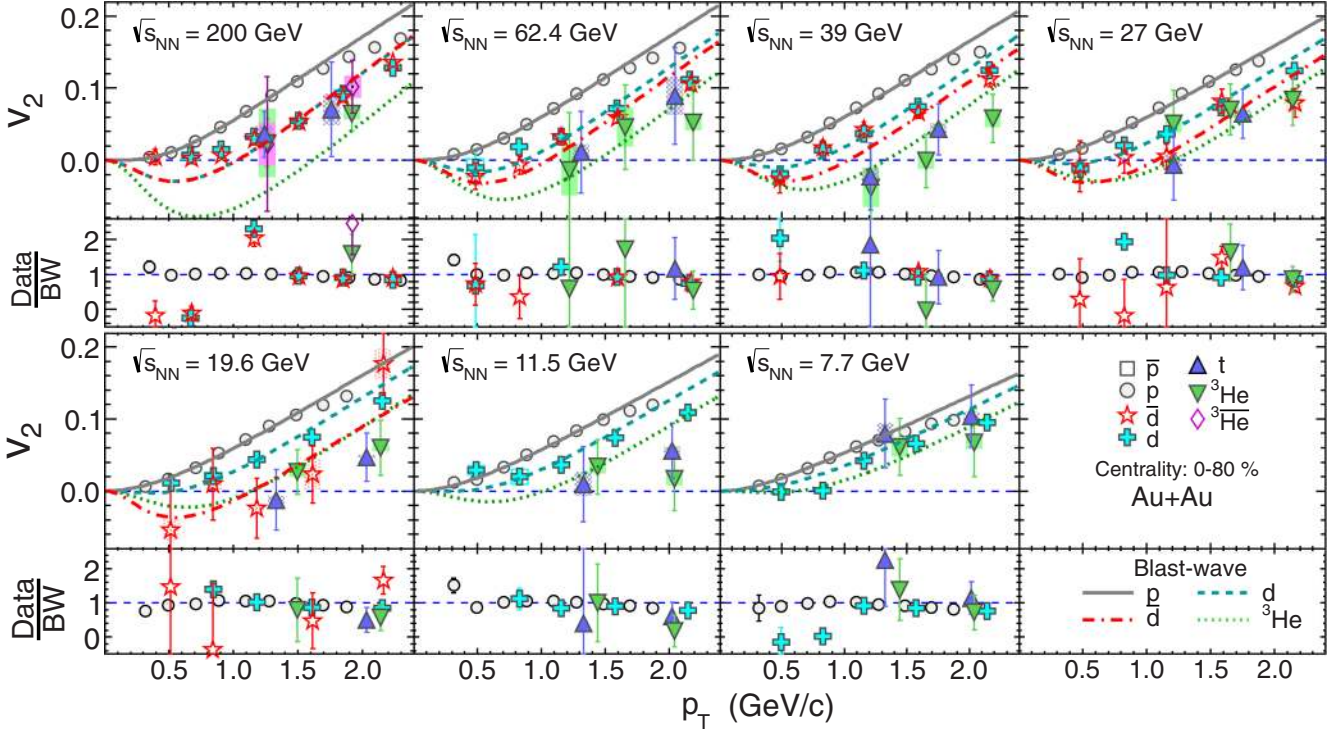
FIG. 8. Blast-wave-model predictions (lines) of v_2 for d, $\overline{d}$, t, ^{3}He ($^3\overline{\text{He}}$) compared with the data for minimum-bias Au + Au collisions. The blast-wave model and parameter values have been used from Ref. [45]. (Some data points in the lower panels are off scale.)

fit parameter values (with $T = 120$ MeV) to check whether the bast-wave model also reproduces the v_2 of light nuclei measured in the data. Figure 8 shows the blast-wave model predictions for light nuclei, along with the measurements. As is evident from Fig. 8, the blast-wave model underpredicts the v_2 of d and $\overline{d}$ at low p_T ($p_T < 1.0$ GeV/c) for most of the collision energies. A similar conclusion for t, ^{3}He ($^3\overline{\text{He}}$) is difficult to make due to their large statistical uncertainty. However, for $\sqrt{s_{NN}} = 200$ GeV, the blast-wave model, with current parametrizations as aforementioned, underestimated the measured v_2 of light nuclei of all species at low p_T ($p_T < 1.0$ GeV/c).

C. Atomic mass number scaling and coalescence model

Figure 9 presents the light-nuclei v_2/A as a function of p_T/A, where A is the atomic mass number of the corresponding light nuclei. The main goal of this study is to understand whether light (anti) nuclei production is consistent with coalescence of (anti) nucleons. The model predicts that, if a composite particle were produced by coalescence of n number of particles that are very close to each other in phase space, then $v_2(p_T)$ of the composite will be n times that of the constituents [46]. In Fig. 9 it is observed that the (anti) nuclei v_2/A closely follows v_2 of p ($\overline{p}$) for p_T/A up to 1.5 GeV/c. The scaling behavior holds ($p_T/A < 1.5$ GeV/c) within 5%–20% for all beam energy range presented. The scaling behavior of these nuclei suggest that d ($\overline{d}$) within $p_T < 3.0$ GeV/c and t, ^{3}He ($^3\overline{\text{He}}$) within $p_T < 4.5$ GeV/c might have formed via the coalescence of nucleons (antinucleons).

The low relative production of light nuclei and the scaling behavior of their elliptic flow seems to be favored by the coalescence formalism over the other methods, such as thermal production which can reproduce the measured particle ratios in data [47,48]. Because protons and neutrons have the same v_2 expected from NCQ scaling, then we can readily see that the v_2 of t and ^{3}He will be the same as they have the same atomic mass number ($A = 3$). We find that, within statistical errors, our measurement of $v_2(p_T)$ for t and ^{3}He confirms this assumption. Although simple A scaling seems to hold for the collision energies presented, the actual mechanism might be a more dynamic process including production and coalescence of nucleons in the local rest frame of the fluid cell. This scenario might give rise to deviations from simple A scaling.

It is arguable that light nuclei could have also formed via coalescence of quarks because the scaling behavior holds when v_2 and p_T are scaled by the number of constituent quarks (e.g., six for d, $\overline{d}$ and nine for t, ^{3}He) instead of mass number. Although this process seems physically acceptable, the survival of light nuclei, with their low binding energies ($\sim$few MeV), is highly unlikely under the high temperatures requisite for dissociating nucleons into quarks and gluons.

To further verify the applicability of nucleon coalescence into light nuclei in heavy-ion collisions, we have run the string-melting version of the A Multi Phase Transport (AMPT, version v1.25t7d) [49] model of the collisions in conjunction with a dynamic coalescence model. The AMPT model has been used to reproduce charged particle multiplicity, transverse momentum spectra at RHIC and the Large Hadron Collider (LHC), as well as v_2 of identified particles at RHIC [49].
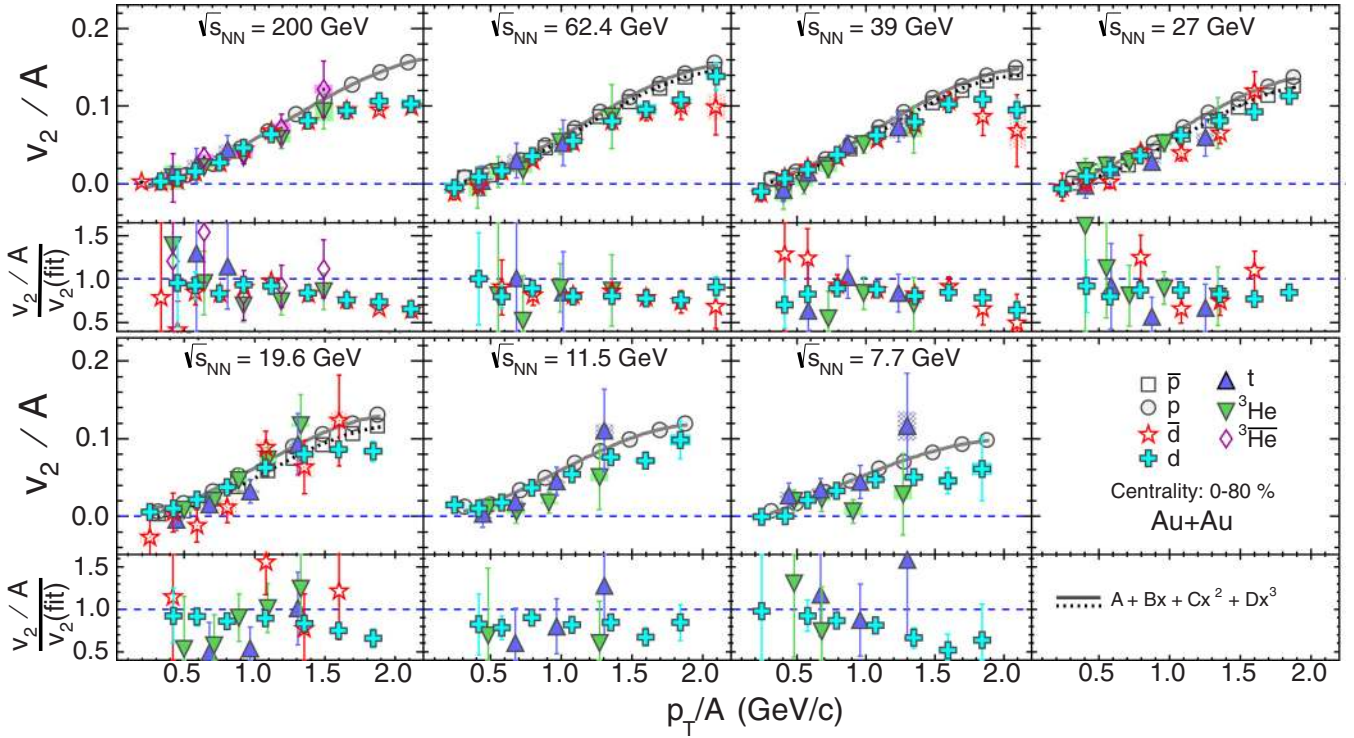
FIG. 9. Atomic mass number (A) scaling of the midrapidity v_2 of p, $\overline{p}$, d, $\overline{d}$, t, ^{3}He, and $^3\overline{\text{He}}$ from minimum-bias Au + Au collisions at $\sqrt{s_{NN}} = 200$, 62.4, 39, 27, 19.6, 11.5, and 7.7 GeV. Gray solid (black dotted) lines correspond to third order polynomial fits to the p ($\overline{p}$) v_2 data. The ratios of $[v_2/A]$/fit for d, $\overline{d}$, t, and ^{3}He are shown in the lower panels at each corresponding collision energy. (Some data points in the lower panels are off scale.)

The dynamic coalescence model has been used extensively at both intermediate [50] and high energies [51]. In this model, the probability for producing a cluster is determined by the overlap of the cluster's Wigner phase-space density with the nucleon phase-space distribution at freeze-out procured from AMPT. For light nuclei, the Wigner phase-space densities are obtained from their internal wave functions, which are taken

to be those of a spherical harmonic oscillator [19,52]. For the coalescence model we have used radii of 1.96, 1.61, and 1.74 fm for d, t, and ^{3}He, respectively [53]. These parameters are kept fixed for the collision-energy range presented. The model's results for v_2 of d, t, and ^{3}He are shown as solid bands in Fig. 10. The data and model agree within errors over nearly all energies and p_T measured, supporting the theory that
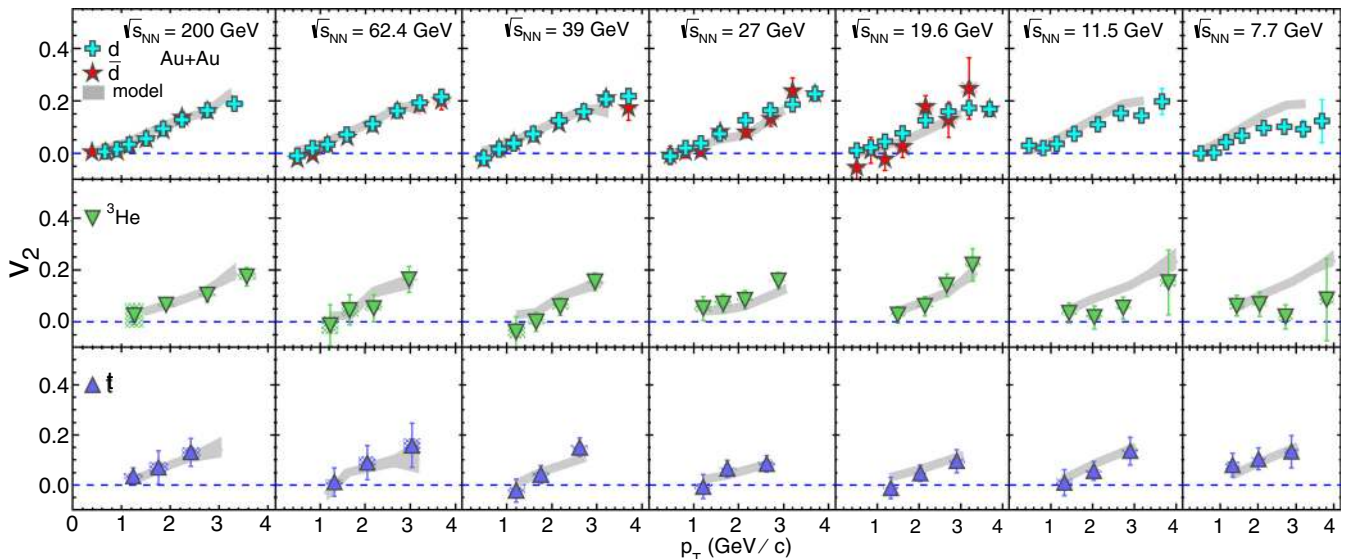

FIG. 10. Midrapidity v_2 of d, t, and ^{3}He are compared with the results of AMPT + coalescence calculations (solid bands).

light nuclei are produced via nucleon coalescence in heavy-ion collisions. Recently, the ALICE collaboration has measured production of d and $\bar{d}$ in Pb + Pb collisions at $\sqrt{s_{NN}} = 2.76$ TeV [54]. In that study, light-nuclei spectra were found to exhibit a significant hardening with increasing centrality. The stiffening of light-nuclei spectra at ALICE could be the result of increased hard scattering, modified fragmentation, or increased radial flow. However, the analysis lacks conclusive evidence regarding the production mechanism of light nuclei in heavy-ion collisions. In the collision-energy range presented in this paper, it seems that nucleonic coalescence might be the leading mechanism of light-nuclei formation in heavy-ion collisions.

IV. SUMMARY

Measurements of the second-order azimuthal anisotropy, $v_2(p_T)$ at midrapidity ($|y| < 1.0$) have been presented for light nuclei d, t, ^{3}He (for $\sqrt{s_{NN}} = 200, 62.4, 39, 27, 19.6, 11.5$, and 7.7 GeV), and antinuclei $\bar{d}$ ($\sqrt{s_{NN}} = 19.6-200$ GeV) and $^3\overline{\text{He}}$ ($\sqrt{s_{NN}} = 200$ GeV). Similar to hadrons over the measured p_T range, light-(anti)nuclei $v_2(p_T)$ show a monotonic rise with increasing p_T, mass ordering at low p_T, and a reduction for more central collisions. It is observed that v_2 of nuclei and antinuclei are of similar magnitude for $\sqrt{s_{NN}} = 39$ GeV and above. The difference Δv_2 between d and $\bar{d}$ is found to be always positive within the statistical uncertainty. Δv_2 of light nuclei seems to qualitatively follow the difference between p and $\bar{p}$ as a function of collision energy. The blast-wave model parametrization, used for reproduction of the identified particle v_2 in the similar beam energies, is found to underestimate the light-nuclei v_2 in the low-p_T (<1.0 GeV) region but approximately reproduces the measurements at intermediate p_T. Within the statistical uncertainty ^{3}He and t nuclei have almost similar magnitude of v_2 for all collision energies. The fact that all the light-nuclei v_2 generally follow an atomic mass number scaling indicates that the coalescence of nucleons might be the underlying mechanism of light-nuclei formation in high-energy heavy-ion collisions. This observation is further corroborated by carrying out a model-based study of nuclei v_2 using a transport-plus-coalescence model, which reproduces well the light-nuclei v_2 measured in the data except for the extremely low collision energies.

[1] M. A. Stephanov, K. Rajagopal, and E. V. Shuryak, Phys. Rev. Lett. **81**, 4816 (1998); Phys. Rev. D **60**, 114028 (1999); M. A. Stephanov, PoS **LAT2006**, 024 (2006); K. Fukushima and T. Hatsuda, Rep. Prog. Phys. **74**, 014001 (2010).

[2] I. Arsene *et al.* (BRAHMS Collaboration), Nucl. Phys. A **757**, 1 (2005); B. B. Back *et al.* (PHOBOS Collaboration), *ibid.* **757**, 28 (2005); J. Adams *et al.* (STAR Collaboration), *ibid.* **757**, 102 (2005); K. Adcox *et al.* (PHENIX Collaboration), *ibid.* **757**, 184 (2005).

[3] L. Adamczyk *et al.* (STAR Collaboration), Phys. Rev. C **86**, 054908 (2012).

[4] L. Adamczyk *et al.* (STAR Collaboration), Phys. Rev. C **88**, 014902 (2013).

[5] L. Adamczyk *et al.* (STAR Collaboration), Phys. Rev. Lett. **110**, 142301 (2013).

[6] L. Adamczyk *et al.* (STAR Collaboration), Phys. Rev. C **93**, 014907 (2016).

[7] A. Adare *et al.* (PHENIX Collaboration), arXiv:1410.2559.

[8] A. Adare *et al.* (PHENIX Collaboration), Phys. Rev. C **93**, 011901 (2016).

[9] L. Adamczyk *et al.* (STAR Collaboration), Phys. Rev. Lett. **116**, 062301 (2016).

[10] S. A. Voloshin, Nucl. Phys. A **715**, 379c (2003).

[11] D. Molnar and S. A. Voloshin, Phys. Rev. Lett. **91**, 092301 (2003).

[12] J. Adams *et al.* (STAR Collaboration), Phys. Rev. Lett. **95**, 122301 (2005).

[13] X. Dong *et al.*, Phys. Lett. B **597**, 328 (2004); Nu Xu, J. Phys. Conf. Ser. **50**, 243 (2006).

[14] R. A. Lacey and A. Taranenko, PoS **CFRNC2006**, 021 (2006).

[15] A. Adare *et al.* (PHENIX Collaboration), Phys. Rev. C **85**, 064914 (2012).

[16] B. Abelev *et al.* (ALICE Collaboration), J. High Energy Phys. 06 (2015) 190.

[17] V. Greco, C. M. Ko, and P. Lévai, Phys. Rev. C **68**, 034904 (2003).

[18] H. H. Gutbrod *et al.*, Phys. Rev. Lett. **37**, 667 (1976).

[19] R. Scheibl and U. Heinz, Phys. Rev. C **59**, 1585 (1999).

[20] H. Sato and K. Yazaki, Phys. Lett. B **98**, 153 (1981).

[21] S. T. Butler and C. A. Pearson, Phys. Rev. **129**, 836 (1963).

[22] W. J. Llope *et al.*, Phys. Rev. C **52**, 2004 (1995).

[23] S. Afanasiev *et al.* (PHENIX Collaboration), Phys. Rev. Lett. **99**, 052301 (2007).

[24] B. I. Abelev *et al.* (STAR Collaboration), arXiv:0909.0566v1.

[25] C. Jena (STAR Collaboration), arXiv:1101.4196.

[26] H. Bichsel, Nucl. Instrum. Methods Phys. Res., Sect. A **562**, 154 (2006).

[27] K. H. Ackermann *et al.* (STAR Collaboration), Nucl. Instrum. Methods Phys. Res., Sect. A **499**, 624 (2003).

[28] M. Anderson *et al.* (STAR Collaboration), Nucl. Instrum. Methods Phys. Res., Sect. A **499**, 659 (2003).

[29] W. J. Llope, Nucl. Instrum. Methods Phys. Res., Sect. B **241**, 306 (2005); Nucl. Instrum. Methods Phys. Res., Sect. A **661**, S110 (2012).

[30] W. J. Llope *et al.*, Nucl. Instrum. Methods Phys. Res., Sect. A **759**, 23 (2014).

[31] C. Adler *et al.* (STAR Collaboration), Nucl. Instrum. Methods Phys. Res., Sect. A **470**, 488 (2001).

[32] C. A. Whitten, Jr., AIP Conf. Proc. **980**, 390 (2008); J. Kiryluk, arXiv:hep-ex/0501072.

[33] D. Kharzeev and M. Nardi, Phys. Lett. B **507**, 121 (2001).

[34] A. M. Poskanzer and S. A. Voloshin, Phys. Rev. C **58**, 1671 (1998).

[35] S. A. Voloshin, A. M. Poskanzer, and R. Snellings, Collective phenomena in non-central nuclear collisions, in *Relativistic Heavy Ion Physics*, Landolt-Börnstein Series (Springer-Verlag, Berlin, 2010), Vol. 23, p. 293.

[36] P. Danielewicz *et al.*, Phys. Rev. C **38**, 120 (1988); J. Barrette *et al.* (E877 Collaboration), *ibid.* **55**, 1420 (1997); **56**, 3254 (1997).

[37] B. I. Abelev *et al.* (STAR Collaboration), Phys. Rev. C **81**, 044902 (2010).

[38] H. Masui, A. Schmah, and A. M. Poskanzer, Nucl. Instrum. Methods Phys. Res., Sect. A **833**, 181 (2016).

[39] P. Huovinen, P. F. Kolb, U. W. Heinz, P. V. Ruuskanen, and S. A. Voloshin, Phys. Lett. B **503**, 58 (2001).

[40] G. D. Westfall *et al.*, Phys. Rev. Lett. **37**, 1202 (1976).

[41] P. J. Siemens and J. O. Rasmussen, Phys. Rev. Lett. **42**, 880 (1979).

[42] J. P. Bondorf, S. I. A. Garpman, and J. Zimanyi, Nucl. Phys. A **296**, 320 (1978).

[43] E. Schnedermann, J. Sollfrank, and U. Heinz, Phys. Rev. C **48**, 2462 (1993).

[44] C. Adler *et al.* (STAR Collaboration), Phys. Rev. Lett. **87**, 182301 (2001).

[45] X. Sun, H. Masui, A. M. Poskanzer, and A. Schmah, Phys. Rev. C **91**, 024903 (2015).

[46] T. Z. Yan *et al.*, Phys. Lett. B **638**, 50 (2006).

[47] S. Chatterjee and B. Mohanty, Phys. Rev. C **90**, 034908 (2014).

[48] A. Andronic, P. Braun-Munzinger, J. Stachel, and H. Stöcker, Phys. Lett. B **697**, 203 (2011).

[49] Z. W. Lin, C. M. Ko, B. A. Li, B. Zhang, and S. Pal, Phys. Rev. C **72**, 064901 (2005).

[50] M. Gyulassy, K. Frankel, and E. A. Remler, Nucl. Phys. A **402**, 596 (1983); J. Aichelin, A. Rosenhauer, G. Peilert, H. Stoecker, and W. Greiner, Phys. Rev. Lett. **58**, 1926 (1987); V. Koch *et al.*, Phys. Lett. B **241**, 174 (1990); L. W. Chen, C. M. Ko, and B. A. Li, Phys. Rev. C **68**, 017601 (2003).

[51] J. L. Nagle, B. S. Kumar, D. Kusnezov, H. Sorge, and R. Mattiello, Phys. Rev. C **53**, 367 (1996); R. Mattiello, H. Sorge, H. Stöcker, and W. Greiner, *ibid.* **55**, 1443 (1997); L. W. Chen and C. M. Ko, *ibid.* **73**, 044903 (2006).

[52] A. T. M. Aerts and C. B. Dover, Phys. Rev. D **28**, 450 (1983).

[53] Lie-Wen Chen, C. M. Ko, and Bao-An Li, Nucl. Phys. A **729**, 809 (2003).

[54] J. Adam *et al.* (ALICE Collaboration), Phys. Rev. C **93**, 024917 (2016).